Atomistic simulation of structure and dynamics of columnar phases of hexabenzocoronene derivatives

Denis Andrienko, Valentina Marcon,[a] and Kurt Kremer
Max-Planck-Institut für Polymerforschung, Ackermannweg 10, 55128 Mainz, Germany

Using atomistic molecular dynamics simulations we study solid and liquid crystalline columnar discotic phases formed by alkyl-substituted hexabenzocoronene mesogens. Correlations between the molecular structure, packing, and dynamical properties of these materials are established. © *2006 American Institute of Physics*. [DOI: 10.1063/1.2354156]

I. INTRODUCTION

Most discotic thermotropic liquid crystals are formed by flat molecules with a central aromatic core and several aliphatic chains attached at the edges.[1,2] The size and shape of the core can be varied, as well as the length and structure of the side chains, which helps to control the functional properties of these materials.[3] Triphenylenes,[4] hexabenzocoronenes (HBCs), and their derivatives[3,5] are the most frequently studied examples of discotics.

The main feature of discotic liquid crystals is that they form columnar phases, where the molecules stack on top of each other and the columns arrange in a regular lattice[1] as sketched in Fig. 1. The self-organization into stacks with aromatic cores surrounded by saturated hydrocarbons results in predominantly one-dimensional charge transport within the core, along the columns.[6,7] By modifying the periphery and the shape of the core it is possible to obtain materials with small charge trapping and recombination.

Conducting properties of discotics are useful for various photovoltaic devices, in particular, solar cells and plastic organic field-effect transistors. In solar cells it is important that the charges can find a direct percolation path to the electrodes without being trapped in an island of the material. Therefore, the *morphology* of the conducting film has a big impact on the efficiency of the device.[8–10] The ideal structure is an aligned discotic liquid crystal with the columns perpendicular (solar cell) or parallel (field-effect transistor) to the substrate.

The spacial arrangement of stacks is, however, never perfect: the columns can be misaligned, tilted, or form various types of topological defects. In addition, the local alignment of molecules in columns can be different for different compounds, changing the overlap of the π orbitals and affecting the efficiency of the charge transport in a single column. It is, therefore, important to control both the local alignment of the molecules in the columns and the global arrangement of the columns in the mesophase. Since these properties are fixed by the molecular architecture and processing conditions, the main task of synthetic chemistry is to synthesize compounds which have various shapes of the core

and different peripheries, to optimize the conducting properties of the mesophase. One should keep in mind, however, that perfect arrangement of the molecules itself does not always mean optimal conducting properties: overlap of the π-π orbitals, splitting of the highest occupied molecular orbital (HOMO) level, etc., affect the efficiency of the charge transport and should be taken into account.

The actual synthesis of each particular compound can involve many stages and be rather time consuming. It is thus helpful to get an insight into the mesophase properties prior to the actual synthesis. For this purpose various computer simulation techniques can be used. Depending on the length and time scales several techniques can be involved: for example, quantum chemistry calculations are used to study the adsorption of molecules on electrodes and the charge transfer mechanisms;[11] molecular dynamics (MD) simulations with atomistic force fields are employed to calculate local properties, such as order parameters and molecular arrangement;[12–15] finally, coarse-grained simulations are successful in studying the morphology of the bulk material, global arrangement of columns, generic phase diagrams, and defects.[16–22]

The number of computer simulations so far performed on discotic materials, is, however, relatively small and most of them are done using idealized model potentials.[18–21] However, a closer contact with real experiments requires more chemical details to be put in. Up to now, there have only been a few attempts to perform atomistic simulations of bulk discotic liquid crystals, mostly on the triphenylene-based
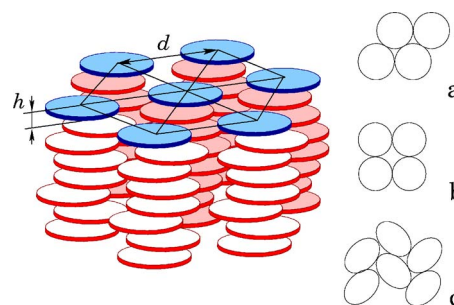

FIG. 1. (Color online) Columnar phase formed by the disk-shaped molecules and the most common arrangements of columns in two-dimensional lattices: (a) hexagonal, (b) rectangular, and (c) herringbone.
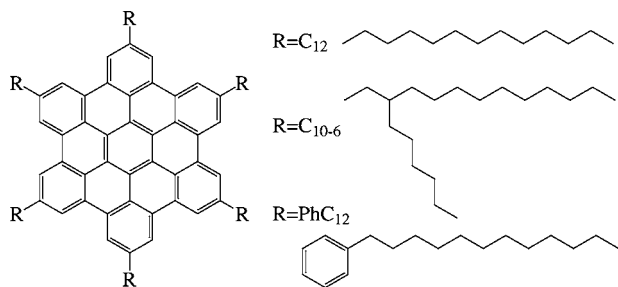
[a] Electronic mail: marcon@mpip-mainz.mpg.de

FIG. 2. Studied derivatives of hexabenzocoronene: $R=C_{10}$, C_{12}, C_{14}, C_{16}, C_{10-6}, PhC_{12}. Only $R=C_{12}$, C_{10-6}, and PhC_{12} are shown.

systems with a small aromatic core.[15] Derivatives of hexa-benzocoronenes are, however, more promising for molecular applications, due to their larger aromatic core and better overlap of the π orbitals. The atomistic simulation of the structure and dynamics of the derivatives of hexabenzocoronenes is the subject of the present paper.

II. STUDIED SYSTEMS AND COMPUTATIONAL DETAILS

The molecular structures of the studied hexabenzocoronene derivatives are shown in Fig. 2. All of them consist of a central flat aromatic core and six side chains. We considered several types of side chains: alkyl chains of different lengths, C_n, with $n=10,12,14,16$; branched side chains, C_{10-6}; and dodecylphenyl-substituted PhC_{12}. The choice of systems is based on the availability of experimental data (wide angle x-ray scattering, solid-state NMR, and differential scanning calorimetry[6,23–26]).

A. Model potential

In our simulation we adopt the united atom approach, and consider explicitly only the hydrogen atoms belonging to the aromatic rings of the central core, since the charge on these hydrogens is responsible for the multipole of the core of the molecule and the interaction of the side chains with aromatic cores is not important in the columnar phase. To describe the intermolecular and intramolecular interactions, we define eight different types of atoms (see Fig. 3 and Table I): aromatic carbons of the central ring (C_B), aromatic carbons bonded to the hydrogens (C_H), hydrogens (H), aliphatic carbons representing either a methylene group (C_2), terminal
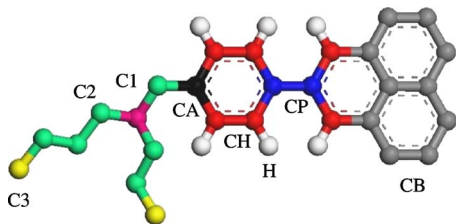

FIG. 3. (Color online) Molecular fragment which illustrates the atom types used in the MD simulations. Methylene and methyl groups of the aliphatic chains are considered as one interaction site, according to the united atom approach.

TABLE I. Atom types and parameters of nonbonded interactions taken from the OLPS force field. Atom types correspond to those shown in Fig. 3.

Atom	Mass (a.u.)	$q(e)$	ϵ (kJ mol^{-1})	σ (nm)
C_A, C_B, C_P	12.011	0	0.293	0.355
C_H	12.011	−0.115	0.293	0.355
H	1.008	0.115	0.125	0.242
C_1	13.019	0	0.450	0.3905
C_2	14.027	0	0.494	0.3905
C_3	15.035	0	0.732	0.3905

methyl group (C_3), or a junction (C_1), and aromatic carbons bonding either alkyl chain (C_A) or two aromatic subsystems (C_P).

The potential energy of the system is then given by the following sum of contributions:

$$E = \sum_{bonds} \frac{1}{2} K_b (r - r_0)^2 + \sum_{angles} \frac{1}{2} K_q (\theta - \theta_0)^2$$
$$+ \sum_{dihedrals} \sum_{n=1}^{3} \left\{ \frac{V_n}{2} [1 + (-1)^{n+1} \cos n\phi] \right\}$$
$$+ \sum_{impropers} K_d (\psi - \psi_0)^2 + \sum_i \sum_{j>i} \left\{ \frac{1}{4\pi\epsilon\epsilon_0} \frac{q_i q_j}{r_{ij}} \right.$$
$$\left. + 4\epsilon_{ij} \left[\left(\frac{\sigma_{ij}}{r_{ij}} \right)^{12} - \left(\frac{\sigma_{ij}}{r_{ij}} \right)^6 \right] \right\}. \quad (1)$$

The first four terms in Eq. (1) correspond to the energy due to the bonded interactions: harmonic bonds (1-2 interactions), angles (1-3 interactions), and torsions, which include Ryckaert-Bellemans and improper dihedrals (1-4 interactions). The potential parameters are taken from the AMBER (Ref. 27) and OPLS (Refs. 28–30) force fields and are listed in Tables I–IV.

The last double sum in Eq. (1) is due to the nonbonded interactions. It is given by the Coulomb and Lennard-Jones terms with q_i the effective charges and ϵ_{ij} and σ_{ij} the well depth and contact distance of the sites i and j. The interaction potential between two atoms of the same type has its own set of parameters q_i, ϵ_{ii}, σ_{ii}, whereas between two different atoms the interaction energy $\epsilon_{ij} = \sqrt{\epsilon_{ii}\epsilon_{jj}}$ is given by the geometrical mean of the two pairs of atoms and the arithmetic average for the lengths $\sigma_{ij} = \frac{1}{2}(\sigma_{ii} + \sigma_{jj})$ (Lorentz-Berthelot mixing rules). Note that 1-2, 1-3, and also 1-4 interactions do not contribute to the above double sum. Furthermore, nonbonded interactions between pairs of sites belonging to the central aromatic core have been excluded. The parameters of

TABLE II. Force constants and equilibrium bond distances. Atom types correspond to those shown in Fig. 3. Parentheses mean that no differences have been made between the included types of atoms.

Bond	b_0 (nm)	K_b (kJ mol^{-1} nm^{-2})
$C_{[A,B,H,P]}-C_{[A,B,H,P]}$	0.139	413 400
$C_{[2,3]}-C_{[2,3]}$	0.153	334 720
C_H-H	0.108	418 400
C_1-C_2	0.153	334 720

TABLE III. Force constants and equilibrium angles. Atom types correspond to those shown in Fig. 3. Parentheses mean that no differences have been made between the included types of atoms.

Angle	θ (degree)	K_θ (kJ mol^{-1} rad^{-2})
$C_{[B,H]}-C_{[B,H,2]}-C_{[B,H,2]}$	120	527
$C_2-C_2-C_{[2,3]}$	109.47	502.1
$C_B-C_2-C_1$	120	527
$C_1-C_2-C_2$	109.47	502.1

the nonbonded interactions are given in Table I. Note that a similar model has already been used to study hexakis(pentyloxy)triphenylenes.[15]

B. Computational details

We simulated systems of 160 molecules, arranged in columns of ten molecules each. The initial configuration was either a hexagonal ($T=400$ K) or rectangular ($T=300$ K) arrangement of the columns (see Fig 1). The distance between the columns and between the molecules in the columns has been slightly increased to avoid site superposition. After the energy minimization, a short equilibrating run (4 ns) was performed at a constant pressure $P=0.1$ MPa and a constant temperature $T=200$ K. Quenching the system at a lower temperature helps to avoid trapping it in a disordered (nonequilibrium) state from the very beginning. We used the method of Berendsen *et al.*[31] with anisotropic pressure coupling. The simulation box angles were fixed at 90°. The electrostatic interactions were treated with the smooth particle-mesh Ewald (PME) method[32] (spacing for PME grid 0.12 nm, cutoff 0.9 nm). The time step of 2 fs was used to integrate equations of motion using the velocity Verlet algorithm with a 0.9 nm cutoff for short-range interactions. All calculations were performed with the parallel version of the GROMACS program.[33] Bond lengths were constrained using the LINCS algorithm[34] provided by GROMACS.

After the equilibration, the simulation box was a parallelepiped of edges L_x, L_y, and L_z, with $L_x/L_y=\sqrt{3}/2$ or $L_x/L_y=1$, depending on the arrangement of the columns (hexagonal or rectangular lattice).

TABLE IV. Parameters of the torsional potential. X can be an aromatic carbon or a carbon bonded to a hydrogen. Parentheses mean that no differences have been made between the included types of atoms. V_1, V_2, and V_3 are given in kJ mol^{-1} for Ryckaert-Bellemans dihedrals and in kJ mol^{-1} rad^{-2} for improper dihedrals. The main task of improper dihedrals with C_H atom type is to keep the corresponding atoms in a plane. The C1–C2–C2–C2 improper constrains the tertiary carbon C1 to tetrahedrality. Atom types correspond to those shown in Fig. 3.

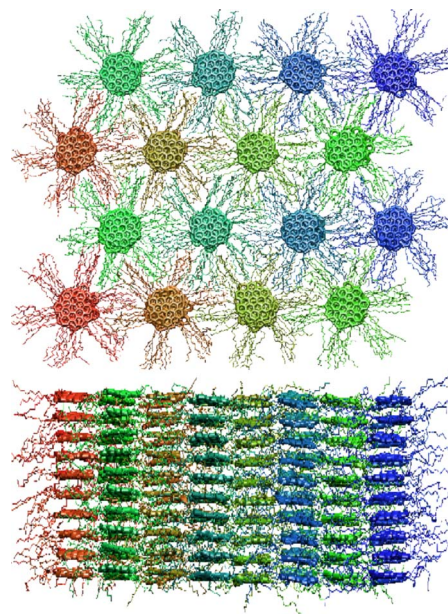| Dihedral	V_1	V_2	V_3
$X-C_{[A,B,P,H]}-C_{[A,B,P,H]}-X$	0.0	121.34	0.0
$C_{[B,2]}-C_{[1,2]}-C_2-C_{[2,3]}$	5.9	−1.14	13.16
Improper	K_d	ψ_0	
$C_P-C_H-C_H-C_P$	167.4	0	
$C_H-C_H-C_A-H$	167.4	0	
$C_H-C_P-C_{[H,B]}-H$	167.4	0	
C1–C2–C2–C2	334.8	35.26	

FIG. 4. (Color online) MD simulation results: snapshot of the system with the C$_{12}$ side chains. Aromatic cores are highlighted. Both top and side views are shown. $T=400$ K, $P=0.1$ MPa. Columns are printed in different arbitrary colors so they can be distinguished in the side view.

The production run (100 ns) was performed at a constant pressure ($P=0.1$ MPa) and temperature fixed using the method of Berendsen *et al.* with time constant $\tau_p=5$ ps and compressibility 4.5×10^{-5} bar^{-1} (both isotropic). Two representative temperatures were chosen: $T=400$ K and $T=300$ K. A 100 ns run took about two-weeks on eight Opteron processors at 2.2 GHz.

III. RESULTS AND DISCUSSION

An equilibrated snapshot of one of the systems at $T=400$ K is shown in Fig. 4. One can see that the aromatic cores are well aligned and the columns are arranged in an almost perfect hexagonal lattice, with the axially symmetric distribution of the side chains. At $T=300$ K the columns are arranged in a rectangular lattice and the cores are also well aligned. To further quantify the arrangement of the molecules we calculated their orientational ordering as well as several positional distribution functions.

A. Orientational order

To calculate the orientational order parameter of the columnar mesophase we considered only the aromatic cores of the molecules. The plane of the core was specified by the six vectors connecting the six C_A atoms. The vector $\boldsymbol{u}^{(i)}$ was then defined as an average of the six normals obtained by the cross product of every pair of two neighboring C_A-C_A vectors. We calculated the orientational order tensor for each column and for the whole system

$$Q_{\alpha\beta} = \left\langle \frac{1}{N} \sum_{i=1}^{N} \left(\frac{3}{2} u_\alpha^{(i)} u_\beta^{(i)} - \frac{1}{2} \delta_{\alpha\beta} \right) \right\rangle, \quad (2)$$

where $\boldsymbol{u}^{(i)}$ is a unit vector normal to the ith aromatic core, and N is the number of molecules in a single column or in
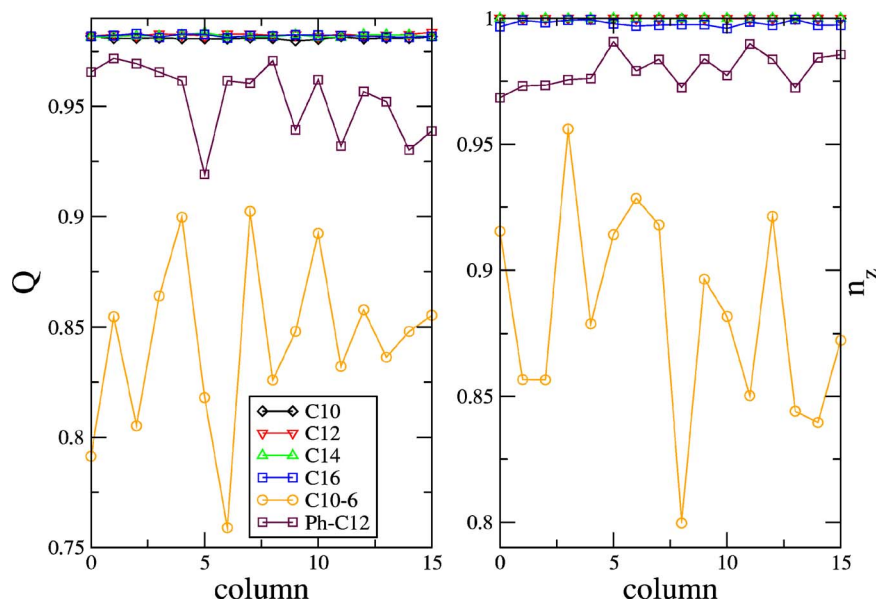
FIG. 5. (Color online) Order parameter Q and the z component of the director (average tilt in the column) as a function of column number. $T = 400$ K.

the whole system; correspondingly, the summation is performed either over a single column or over the whole system. $\langle\cdots\rangle$ denotes the time average. Diagonalizing this tensor we obtain the order parameter Q, which is the largest eigenvalue of $Q_{\alpha\beta}$, and the average orientation of the molecules, or director $\boldsymbol{n}$ which is the eigenvector corresponding to the largest eigenvalue Q. $Q=1$ implies perfect alignment of molecules in the column (all unit vectors parallel to each other), and $Q=0$ corresponds to the isotropic angular distribution of the unit vectors.

The order parameter Q and the average tilt angle of the unit vector $\boldsymbol{n}$ (given by the projection onto the z axis) are summarized in Fig. 5. It is clear that the systems with linear side chains $C_{10}-C_{16}$ are well ordered: the order parameter is close to its maximum value, $Q=1$; in addition, there is no tilt of the molecules in the columns. The system with the dodecylphenyl-substituted side chains, PhC_{12}, has slightly lower ordering (but still rather high, $Q\approx0.95$) and a small average tilt of the molecules in the columns. Finally, the system with the branched chains, C_{10-6}, has the worst ordering: the order parameter is quite low and varies much from column to column; there is also a significant tilt of the molecules in the columns. As can be seen in Table V, in the case of linear chains, the values of the order parameter Q at $T=300$ K are identical to the one at $T=400$ K, while the PhC_{12} shows a bigger disorder; the C_{10-6} becomes more ordered with the decrease in temperature.

B. Positional order

To characterize the bulk structure of the columnar phase, we have calculated two additional correlation functions. The

TABLE V. Summary of the experimental data and simulations. Results of the simulations are marked in bold.

	ρ, 400 K g cm^{-3}	ρ, 300 K g cm^{-3}	d, 400 K nm	d, 300 K nm	h, 400 K nm	h, 300 K nm	Q, 400 K	Q, 300 K
C10-6	**1.001**	**1.044**	**2.54**	**2.62**	**0.363**	**0.331**	**0.85**	**0.97**
C10	**1.043**	**1.087**	**2.57**	**2.26**	**0.367**	**0.363**	**0.98**	**0.98**
C12			2.86[a]	2.38 × 6.1[a,b]	0.355[c]		0.78[c]	
			2.52[c]		0.35[a]		0.84[d]	
	1.027	**1.074**	**2.76**	**2.53**	**0.366**	**0.365**	**0.98**	**0.98**
C14			2.66[c]		0.367[c]			
	1.012	**1.013**	**2.93**	**2.69**	**0.367**	**0.362**	**0.98**	**0.98**
C16			2.66[c]		0.372[c]			
	1.002	**1.002**	**3.09**	**2.87**	**0.368**	**0.363**	**0.98**	**0.98**
Ph-C12			3.4[b]	2.98[b]	0.35[d]		0.93[d]	
					0.346[a]			
	1.062	**1.103**	**3.00**	**2.69**	**0.379**	**0.439**	**0.95**	**0.92**

[a]Reference 23.
[b]This phase has the herringbone symmetry; see Fig. 1.
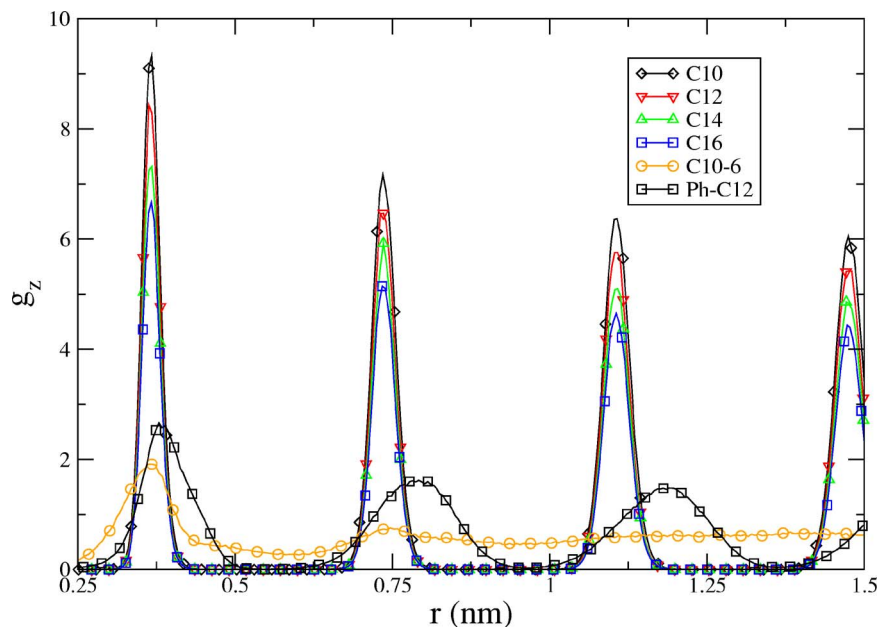[c]Reference 26.
[d]Reference 24.

FIG. 6. (Color online) Probability to find another molecule of the same column at a distance r from the reference molecule. $T=400$ K.

first one, $g_z(r)$, provides information about the arrangement of the molecules in the planes parallel to the director $\boldsymbol{n}$, which in our case is the direction of the columns (along the z axis). In other words, $g_z(r)$, is the probability to find a molecule at a distance $\boldsymbol{n}\cdot\boldsymbol{r}$ from the reference molecule,

$$g_z(r) = \frac{2}{VN}\sum_{\text{columns}}\sum_{i=0}^{N_c}\sum_{j>i}^{N_c} f(\boldsymbol{r},\boldsymbol{n}\cdot\boldsymbol{r}_{ij}). \qquad (3)$$

Here N_c is the number of the molecules in a column, r_{ij} is the distance between the centers of mass of molecules i and j, N is the total number of molecules in the system. f is a binning function, i.e., $f=1$ if $\boldsymbol{n}\cdot\boldsymbol{r}_{ij}\in[r\pm\Delta/2]$, where Δ is the bin size (in our case the number of bins was 400), otherwise $f=0$. $V=\Delta L_x L_y$ is the volume of the bin. Note that the averaging is first performed in each column, and then over the columns, since the columns can diffuse with respect to each other.

Figure 6 shows this distribution function for all studied systems at $T=400$ K. It has a series of narrow peaks, which indicates the ordered stacking of the molecules in the columns. For linear side chains the peaks are sharp and well defined, with a constant distance between molecules in the columns. It is interesting that the separation is not affected by the length of the chain (of course, in the range studied). If a phenyl ring is added, as it is in the case of PhC_{12} or branched side chains, the peaks broaden and shift, indicating a greater disorder of the mesophase. For PhC_{12} the distance between the columns also becomes slightly bigger (see Table V for exact numbers). Simulations at 300 K show, for all the systems investigated, the same distribution functions. This indicates that the difference of 100 K in temperature is not affecting the ordering properties along the columns. Intermolecular separations, which are given by the distances between the neighboring peaks of the distribution function, agree well with the x-ray scattering data and are summarized in Table V.

The second distribution function, g_{xy}, provides information on the arrangement of molecules in planes perpendicular to the director $\boldsymbol{n}$, in the xy plane,

$$g_{xy}(r) = \frac{2}{V(r)N}\sum_{i=0}^{N}\sum_{j>i}^{N} f(\boldsymbol{r},\boldsymbol{n}\times\boldsymbol{r}_{ij}), \qquad (4)$$

where $V(r)=\pi[(r+\Delta)^2-r^2]L_z=\pi\Delta(2r+\Delta)L_z$ is the volume of a cylindrical bin.

The two-dimensional radial distribution function g_{xy} is shown in Fig. 7. It has a large peak around $r=0$, which is because of the molecules in the same column. The other peak is due to the in-plane nearest neighbors and provides us with the lattice constant of hexagonal (or square) arrangement of the columns.

The spacing between in-plane (along the z axis) nearest neighbors increases almost constantly with increasing length of the linear side chains. In the case of branched chains, the position of the peak is almost in the same position as the peak belonging to the simulation of C10, but the peak is broader due to the disorder. For PhC_{12} side chains the peak position is between C14 and C16.

Both the measured values and the values estimated from x-ray diffraction experiments are presented in Table V and are in a fair agreement with each other.

C. Ordering of the side chains

To complete the description of the molecular arrangement in our systems, we also investigated the conformational state of the side chains and the degree of their interdigitation. The conformational behavior of the alkyl side chains is shown in the upper panel of Fig. 8. The distribution functions are given for the C_{12} system. The other systems show identical results. The distribution function of the dihedral CA-C2-C2-C2 (see Fig. 3 for the atom names), that is, the dihedral connecting the core of the molecule with the alkyl side chains, shows that the gauche conformation (at around 60°)
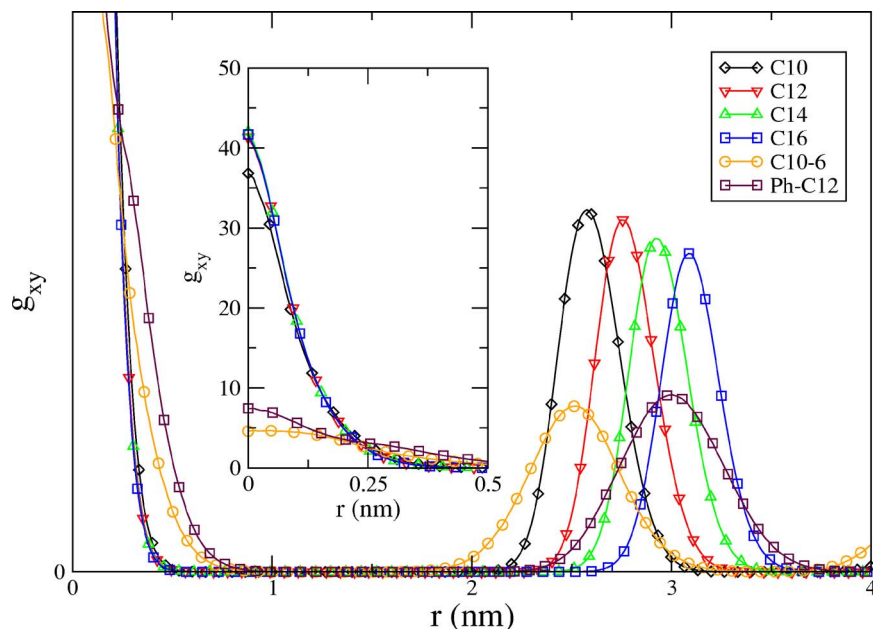
FIG. 7. (Color online) Probability of finding the center of mass of another molecule at a distance r from the reference molecule (two-dimensional radial distribution function). The inset shows the large peak around $r=0$. $T=400$ K.

has the same probability as the *trans* one (at around 180°). The distribution functions of the dihedrals along the alkyl chains (C2-C2-C2-C2) and the terminating one (C2-C2-C2-C3) show that the *trans* state is more probable than the gauche one. For the PhC$_{12}$ system the distribution function of the CH-CP-CP-CH dihedral, shown in the bottom panel of Fig. 8, indicates that the phenyl ring tends to align perpendicularly to the core of the molecule.

We have also evaluated the degree of interdigitation of the side chains. The results, which are shown in Table VI, were evaluated by subtracting the in-plane spacing between molecules in neighboring columns from twice the averaged end-to-end distances of the side chains and a (constant) distance between the center of mass of the molecule and the atom CA (which is approximately 0.57 nm). The longer the side chain is, the higher the percentage of interdigitation is.

D. Translational dynamics

To show that the systems have liquidlike dynamics, we calculated the mean square displacement of the molecular center of mass, along the column direction (z axis),

$$\text{MSD}(t) = \langle [z(t) - z(0)]^2 \rangle, \tag{5}$$

where the average is taken over all molecules.

The resulting profiles are shown in Fig. 9. The log-log profiles show that the mean-squared displacement has $t^{1/2}$ asymptotics for small t which becomes t^1 in the long-time limit. In fact, this type of asymptotics is expected for single-file diffusion,[35,36] when individual particles are unable to pass each other and the particle order remains the same over time. In this case the motion of individual particles requires the collective motion of many other particles in the same direction. In other words, in a one-dimensional geometry the
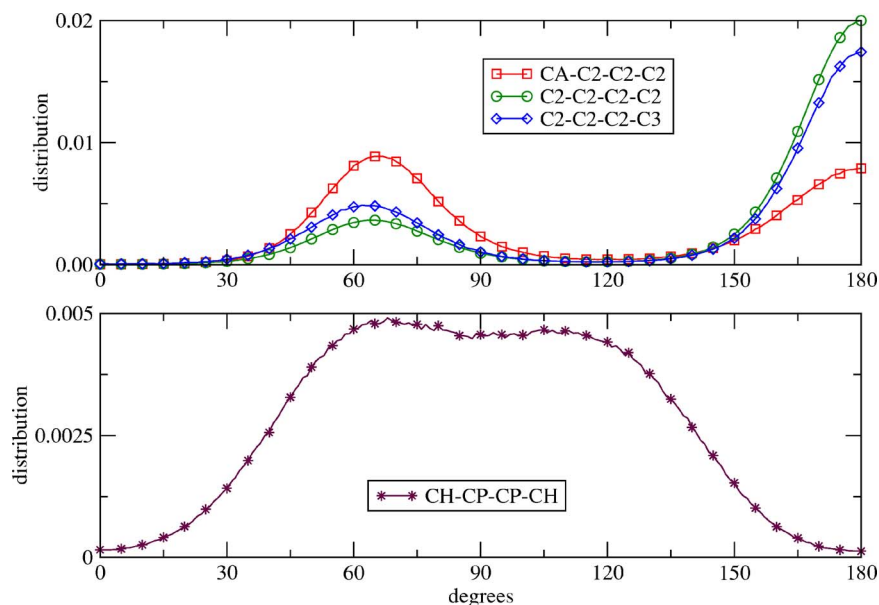

FIG. 8. (Color online) Distribution function of the dihedral angles. The upper panel refers to C$_{12}$ run and the lower one to PhC$_{12}$, both at $T=400$ K.

TABLE VI. Interdigitation of the side chains.

System	End-to-end (nm)	Interdig. (nm)	Interdig. (%)
C_{10}	1.02	0.61	59.8
C_{12}	1.19	0.76	63.8
C_{14}	1.35	0.91	67.4
C_{16}	1.51	1.07	70.9
PhC_{12}	1.50	1.14	76.0

single-particle motion is coupled to the density fluctuations. The fact that we can see the t^1 asymptotics of the mean-squared displacement indicates that we already see diffusion of the column as a whole. Note that in an infinite one-dimensional system there is no diffusion, since the diffusion coefficient scales as $1/N$.

For $T=300$ K the log-log profiles show that the mean-squared displacement has different asymptotics (smaller than $t^{1/2}$) than for $T=400$ K. However, the length of simulation runs does not allow us to conclude whether we have a frozen liquid crystalline state or a solid state.

IV. DISCUSSION AND CONCLUSIONS

We first compare our results to the experimental data available in Refs. 23, 24, and 26.

The x-ray diffraction experiments predict a columnar phase D_h (hexagonal arrangement of columns) at 400 K and D_r (rectangular arrangement) at 300 K. Our simulations show that the systems at 400 K keep the hexagonal symmetry of the lattice during the simulation run. The systems at 300 K stay rectangular for short side chains; for C14, C16 systems the square lattice starts to evolve into a hexagonal one after about 10 ns.

Concerning xy spacing between the columns, the distance increases with the length of the side chains. This trend seems not to be present in experimental data, where, for example, the spacing for C14 and C16 is identical. The deviation between the experimental data and simulation results here is about 10%.

The simulation data concerning the spacing between molecules in the z direction (along the columns) are in fair
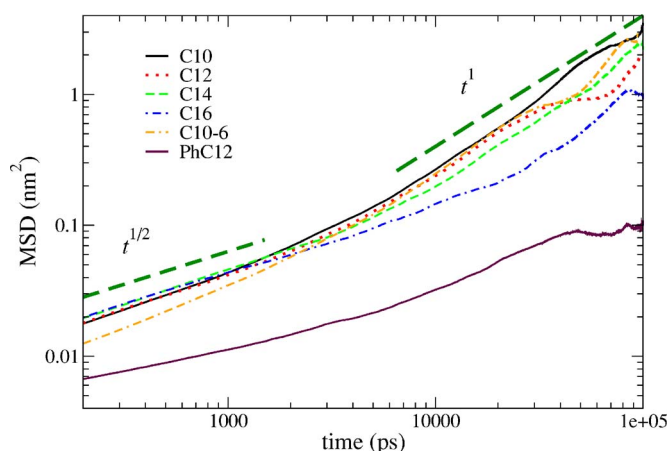
agreement with the experimental results. Maximum deviation for linear chains is about 3%; for the phenyl case there is a deviation of about 10%.

The order parameter obtained in simulations is systematically higher than the one obtained experimentally. Of course, NMR data do not provide exact numbers for the order parameter, rather an estimate of it. However, the main problem is the extremely small size of the studied systems, since periodic boundaries do not allow long-range fluctuations of the molecular order, as well as prohibiting the presence of defects in the system. Therefore, calculated values of the order parameter merely emphasize the difference between different systems, in a qualitative manner: the linear side chains provide perfect ordering of the molecules in the columns; Ph−C_{12} systems show good ordering; branched side chains introduce a significant amount of disorder into the system, often leading to domains of material of different orientation.

Finally, translational dynamics shows typical single-file diffusion behavior. It also indicates that one needs at least 10^5 ps in order to calculate correct dynamic averages and to equilibrate the systems.

The main message of this work is that atomistic molecular dynamics simulations do not really provide complete quantitative description of the columnar mesophases because of the very small time and length scales they can reach. Hence, their main task is to serve as an input to coarse-graining techniques,[37–40] in order to devise appropriate coarse-grained representations. One can then treat much bigger systems on longer time scales. This work is in progress.

ACKNOWLEDGMENTS

FIG. 9. (Color online) Log-log plot of the mean squared displacement. T =400 K.

[1] S. Chandrasekhar and G. S. Ranganath, Rep. Prog. Phys. **53**, 57 (1990).
[2] R. J. Bushby and O. R. Lozman, Curr. Opin. Colloid Interface Sci. **7**, 343 (2002).
[3] J. D. Brand, C. Kubel, S. Ito, and K. Müllen, Chem. Mater. **12**, 1638 (2000).
[4] S. Kumar, Liq. Cryst. **31**, 1037 (2004).
[5] M. Müller, C. Kübel, and K. Müllen, Chem.-Eur. J. **4**, 2099 (1998).
[6] A. M. van de Craats, J. M. Warman, A. Fechtenkotter, J. D. Brand, M. A. Harbison, and K. Müllen, Adv. Mater. (Weinheim, Ger.) **11**, 1469 (1999).
[7] L. Schmidt-Mende, A. Fechtenkotter, K. Müllen, E. Moons, R. H. Friend, and J. D. MacKenzie, Science **293**, 1119 (2001).
[8] J. J. M. Halls, A. C. Arias, J. D. MacKenzie, W. S. Wu, M. Inbasekaran, E. P. Woo, and R. H. Friend, Adv. Mater. (Weinheim, Ger.) **12**, 498 (2000).
[9] S. E. Shaheen, C. J. Brabec, N. S. Sariciftci, F. Padinger, T. Fromherz, and J. C. Hummeleu, Appl. Phys. Lett. **78**, 841 (2001).
[10] A. C. Arias, J. D. MacKenzie, R. Stevenson, J. J. M. Halls, M. Inbasekaran, E. P. Woo, D. Richards, and R. H. Friend, Macromolecules **34**, 6005 (2001).
[11] J. L. Bredas, D. Beljonne, V. Coropceanu, and J. Cornil, Chem. Rev. (Washington, D.C.) **104**, 4971 (2004).
[12] A. Maliniak, J. Chem. Phys. **96**, 2306 (1992).
[13] I. Ono and S. Kondo, Bull. Chem. Soc. Jpn. **65**, 1057 (1992).
[14] F. M. Mulder, J. Stride, S. J. Picken, P. H. J. Kouwer, M. P. de Haas, L. D. A. Siebbeles, and G. J. Kearley, J. Am. Chem. Soc. **125**, 3860 (2003).
[15] G. Cinacchi, R. Colle, and A. Tani, J. Phys. Chem. B **108**, 7969 (2004).
[16] J. A. C. Veerman and D. Frenkel, Phys. Rev. A **45**, 5632 (1992).
[17] A. P. J. Emerson, G. R. Luckhurst, and S. G. Whatling, Mol. Phys. **82**,

113 (1994).

[18] M. A. Bates and G. R. Luckhurst, J. Chem. Phys. **104**, 6696 (1996).

[19] H. Zewdie, Phys. Rev. E **57**, 1793 (1998).

[20] G. Cinacchi and A. Tani, J. Chem. Phys. **117**, 11388 (2002).

[21] D. Caprion, L. Bellier-Castella, and J. P. Ryckaert, Phys. Rev. E **67**, 041703 (2003).

[22] L. Bellier-Castella, D. Caprion, and J. P. Ryckaert, J. Chem. Phys. **121**, 4874 (2004).

[23] I. Fischbach, T. Pakula, P. Minkin, A. Fechtenkotter, K. Müllen, H. W. Spiess, and K. Saalwachter, J. Phys. Chem. B **106**, 6408 (2002).

[24] A. Fechtenkotter, K. Saalwachter, M. A. Harbison, K. Müllen, and H. W. Spiess, Angew. Chem., Int. Ed. **38**, 3039 (1999).

[25] S. P. Brown, I. Schnell, J. D. Brand, K. Müllen, and H. W. Spiess, J. Am. Chem. Soc. **121**, 6712 (1999).

[26] P. Herwig, C. W. Kayser, K. Müllen, and H. W. Spiess, Adv. Mater. (Weinheim, Ger.) **8**, 510 (1996).

[27] W. D. Cornell, P. Cieplak, C. I. Bayly, I. R. Gould, K. M. Merz, D. M. Ferguson, D. C. Spellmeyer, T. Fox, J. W. Caldwell, and P. A. Kollman, J. Am. Chem. Soc. **117**, 5179 (1995).

[28] W. Jorgensen, J. Madura, and C. Swenson, J. Am. Chem. Soc. **106**, 6638 (1984).

[29] W. Jorgensen and D. Severance, J. Am. Chem. Soc. **112**, 4768 (1990).

[30] W. Jorgensen, E. Laird, T. Nguyen, and J. Tirado Rives, J. Comput. Chem. **14**, 206 (1993).

[31] H. J. C. Berendsen, J. P. M. Postma, W. F. van Gunsteren, A. DiNola, and J. R. Haak, J. Chem. Phys. **81**, 3684 (1984).

[32] U. Essmann, L. Perera, M. Berkowitz, T. Darden, H. Lee, and L. Pedersen, J. Chem. Phys. **103**, 8577 (1995).

[33] E. Lindahl, B. Hess, and D. van der Spoel, J. Mol. Model. **7**, 306 (2001).

[34] B. Hess, H. Bekker, H. J. C. Berendsen, and J. G. E. M. Fraaije, J. Comput. Chem. **18**, 1463 (1997).

[35] P. M. Richards, Phys. Rev. B **16**, 1393 (1977).

[36] M. Kollmann, Phys. Rev. Lett. **90**, 180602 (2003).

[37] C. F. Abrams and K. Kremer, Macromolecules **36**, 260 (2003).

[38] F. Müller-Plathe, ChemPhysChem **3**, 754 (2002).

[39] S. Izvekov and A. Violi, J. Chem. Theory Comput. **2**, 504 (2006).

[40] G. Voth, J. Chem. Theory Comput. **2**, 463 (2006).